Infrared nanoimaging of the metal-insulator transition in the charge-density-wave van der Waals material 1T-TaS$_2$

Alex J. Frenzel,[1,*] Alexander S. McLeod,[1,2] Dennis Zi-Ren Wang,[3] Yu Liu,[4] Wenjian Lu,[4] Guangxin Ni,[1] Adam W. Tsen,[2,5] Yuping Sun,[4] Abhay N. Pasupathy,[2] and D. N. Basov[1,2]

[1]*Department of Physics, University of California, San Diego, La Jolla, California 92039, USA*
[2]*Department of Physics, Columbia University, New York, New York 10027, USA*
[3]*Department of Applied Physics and Applied Mathematics, Columbia University, New York, New York 10027, USA*
[4]*Key Laboratory of Materials Physics, Institute of Solid State Physics, Chinese Academy of Sciences, Hefei 230031, Peoples Republic of China*
[5]*Institute for Quantum Computing and Department of Chemistry, University of Waterloo, Waterloo, Ontario N2L 3G1, Canada*

Using scanning near-field optical microscopy at cryogenic temperatures, we explored the first-order metal-insulator transition of exfoliated 1T-TaS$_2$ microcrystals on a SiO$_2$/Si substrate. We clearly observed spatially separated metallic and insulating states during the transition between commensurate and nearly commensurate charge-density-wave phases. The capability to probe electrodynamics on nanometer length scales revealed temperature-dependent electronic properties of the insulating and metallic regions near the transition temperature. At fixed temperature, a remarkably broad spatial boundary between insulating and metallic regions was observed, across which the nano-optical signal smoothly evolved over a length scale of several hundred nanometers. To understand these observations, we performed Ginzburg-Landau calculations to determine the charge-density-wave structure of the domain boundary, which revealed the existence of an intermediate electronic phase with unique properties distinct from the bulk thermodynamic phases.

I. INTRODUCTION

Metallic layered transition metal dichalcogenides exhibit a rich variety of remarkable electronic phenomena, including charge-density-wave ordering [1–7], superconductivity [8–12], metastable states induced optically [13,14] and electrically [15–19], and Mott localization [20,21]. These different phases are highly susceptible to modification by external perturbation, leading to proposals for and demonstrations of novel devices [15–17,22,23]. The 1T structure of TaS$_2$ is distinguished from related compounds by the occurrence of a first-order metal-insulator transition (MIT) concomitant with a nearly commensurate (NC) to commensurate (C) charge-density-wave (CDW) transition [1] [Fig. 1(a)]. This provides a unique opportunity to investigate general properties of temperature-controlled MITs in a clean system beyond the transition metal oxide materials class [24]. Local investigations of oxide MITs on mesoscopic scales have revealed that inhomogeneity is a ubiquitous feature of such transitions and that new electronic phases often arise near the critical temperature [25–30]. While the NC-C MIT in TaS$_2$ has been extensively studied at the atomic scale [3,4,18,19,22,31–33], it remains unexplored on natural length scales associated with the thermodynamic transition.

Scanning near-field optical microscopy [34] (SNOM) has recently emerged as a powerful tool to probe mesoscopic electronic inhomogeneity occurring during phase transitions in strongly correlated oxides [26,28,30,35–37]. This method

has revealed the existence of a correlated metallic state in VO$_2$ (Ref. [26]) and the important role interactions play in driving the MIT in V$_2$O$_3$ (Ref. [30]), but it has not yet been applied to explore mesoscale electrodynamics of the MIT in materials other than oxides. Here, we report infrared nanoimaging (nano-IR) of the metal-insulator transition in thin exfoliated microcrystals of 1T-TaS$_2$ by implementing SNOM at cryogenic temperatures. Upon cooling our micron-scale, nanometer-thick samples through T_c, we observed the formation of insulating regions that grew to surround and engulf the metallic areas as the transition progressed. Our nanoscale resolution allowed us to characterize the local electronic properties of the spatially separated insulating and metallic phases as a function of temperature, revealing temperature-dependent electronic states arising during phase coexistence. The spatial boundary between insulating and metallic regions at fixed temperature was observed to be remarkably wide, indicating the smooth evolution from NC to C charge ordering over hundreds of CDW periods. Through detailed theoretical calculations, we conclude that the observed temperature and spatial dependence of the nano-IR signal reflect the existence of intermediate electronic phases with unique CDW order beyond the NC- and C-CDW states. This latter finding deviates from the expectation for a standard first-order phase transition and sheds new light on the thermodynamics of the MIT in 1T-TaS$_2$.

II. EXPERIMENTAL TECHNIQUE

In our nanoimaging experiments, we irradiated the metallized tip of an atomic force microscope (AFM) with a midinfrared laser beam of frequency $\omega = 1155$ cm^{-1}[photon energy $\hbar\omega \approx 143$ meV; schematic in Fig. 1(b)]. We chose
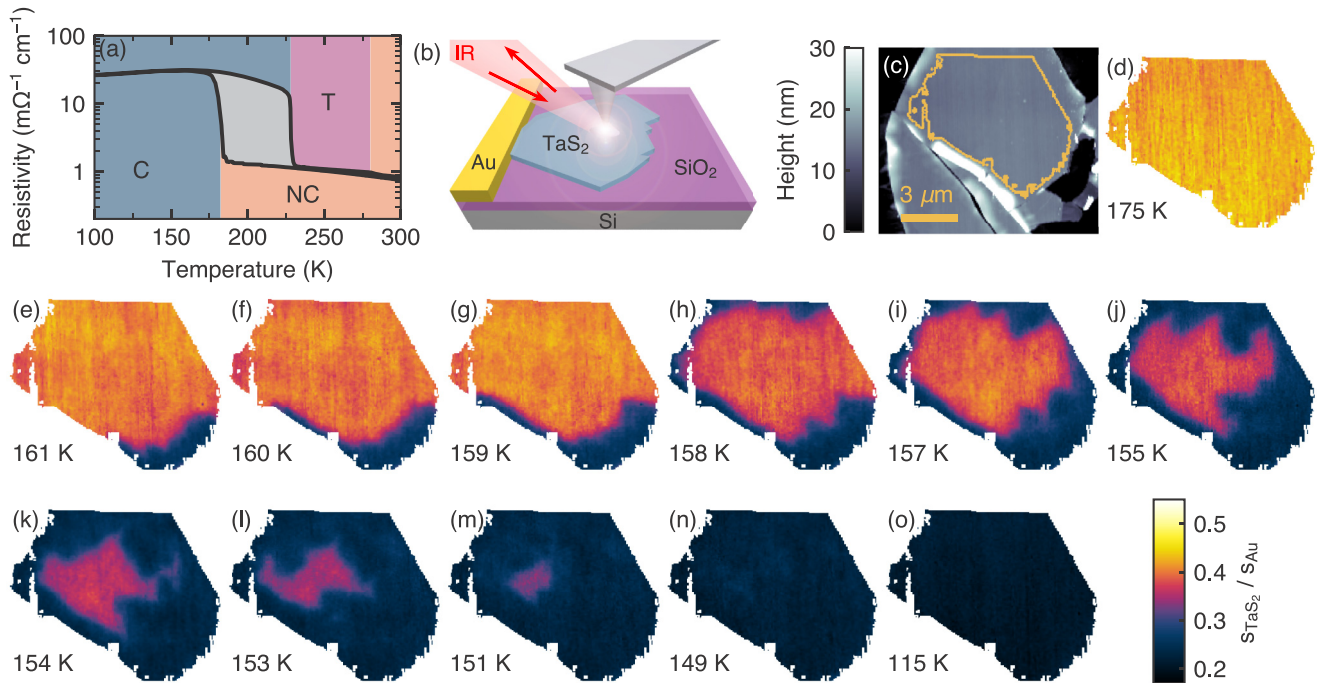
*afrenzel@physics.ucsd.edu

FIG. 1. Imaging the metal-to-insulator transition in a thin microcrystal of $1T$-TaS_2: (a) Resistivity and CDW phase diagram of bulk $1T$-TaS_2. (b) Schematic of the near-field imaging experiment. (c) Sample topography showing the ≈ 12 nm (20 layer) thick microcrystal (the yellow curve shows the outline of the area displayed in the nano-IR images). (d–o) Nano-IR images of metal-to-insulator transition at incident light frequency $\omega = 1155$ cm^{-1}. Insulating regions (blue) first appear around the edges of the microcrystal and grow inwards until the central metallic NC area (yellow and red) vanishes and the entire piece has entered the insulating C phase.

this frequency to maximize the contrast between signal obtained from metallic and insulating regions of the sample (see Ref. [38] for details). The incident laser beam polarized the metallized AFM tip, resulting in partial confinement of the incident electromagnetic wave to a nanoscale volume between the tip apex and sample. Light scattered from this near-field region encoded details of the local optical properties of the sample with spatial resolution set by the AFM tip radius [45]. Experimentally, we recorded the scattered nano-IR amplitude s, which is analogous to the reflectance measured in a conventional optical experiment [38]. In particular, high values of s are expected from metals and lower values are expected for insulators [26]. In contrast to common far-field reflectance, however, s can be obtained with spatial resolution on the order of the AFM tip radius ($r \sim 10$–20 nm), a length scale well below the Abbe diffraction limit for the ≈ 8.7-μm-wavelength probing light [34,46].

III. RESULTS & DISCUSSION

Figure 1(c) displays the topography of a $1T$-TaS_2 microcrystal sample (see Ref. [38] for sample details). The yellow outline shows the boundary of the flat center area, for which nano-IR images are shown in Figs. 1(d)–1(o). We focused on this region to avoid complications arising from varying sample thickness and defects present in other parts of the microcrystal. The signal in the nano-IR images was normalized to a nearby gold pad in order to facilitate quantitative comparison of images recorded at different temperatures. At $T = 175$ K [Fig. 1(d)], when the sample was fully metallic, the center region showed approximately homogeneous signal

of $\approx 0.45\, s_{Au}$, where s_{Au} is the nano-IR signal obtained on gold. Nearing the NC-C transition temperature, a small patch revealing lower signal ($\approx 0.25\, s_{Au}$) appeared at the bottom-right edge of the region [Fig. 1(e)]. As the temperature dropped further, this patch grew and new patches appeared near other microcrystal edges [Figs. 1(f)–1(h)]. Eventually, these patches grew to surround a small high-signal region in the center of the sample [Figs. 1(i)–1(n)], which continued to shrink until the entire microcrystal was in the low-signal state [Fig. 1(o)]. Detailed modeling of the nanoscale light-matter interaction in our experiment allowed us to associate the high-signal regions to the metallic NC phase and low-signal regions to the insulating C phase with confidence [38]. These data therefore unveil the mesoscopic progression of the MIT, revealing previously unobserved emergent length scales associated with the thermodynamics of the transition. While interaction with the substrate may influence the transition characteristics of such a thin microcrystal [9,47], images collected during different cool-downs revealed distinct spatial patterns [38]. This suggests that the length scales are intrinsic and that the metallic puddle shape was set by fluctuations.

We studied the trends exhibited in the nano-IR images of Fig. 1 by examining histogram representations of the normalized nano-IR signal s_{TaS_2}/s_{Au}, shown in Fig. 2(a). At all temperatures for which phase coexistence occurred, the distributions were distinctly bimodal, with a clear peak corresponding to the insulating phase and another well-defined peak representing the metallic phase. The sizable separation between peaks associated with the insulating and metallic phases in the histograms contrasts with the behavior observed in VO_2 and V_2O_3, where signals from the metallic and insu-
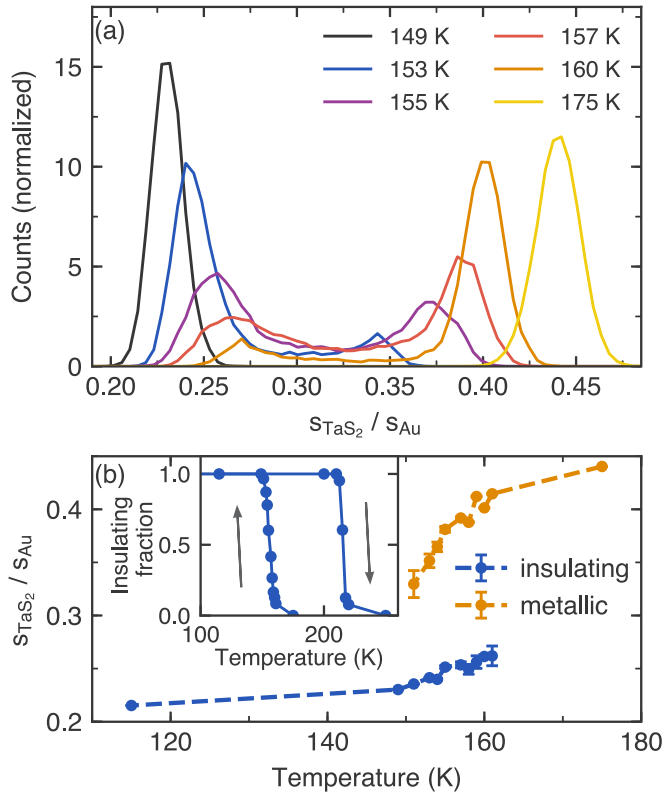
FIG. 2. Quantitative analysis of nanoimaging from Fig. 1: (a) Selected histograms for the cooling transition, showing the evolution of the normalized nano-IR signal with temperature. The bimodal distributions reflect the first-order nature of the transition, while the shift in the peak centers indicates that the underlying electronic properties of the two phases change with temperature. (b) Nano-IR signal as a function of temperature for insulating (blue) and metallic (orange) phases extracted by fitting the histogram distributions, illustrating the change in local optical properties. Inset: insulating fill fraction versus temperature.
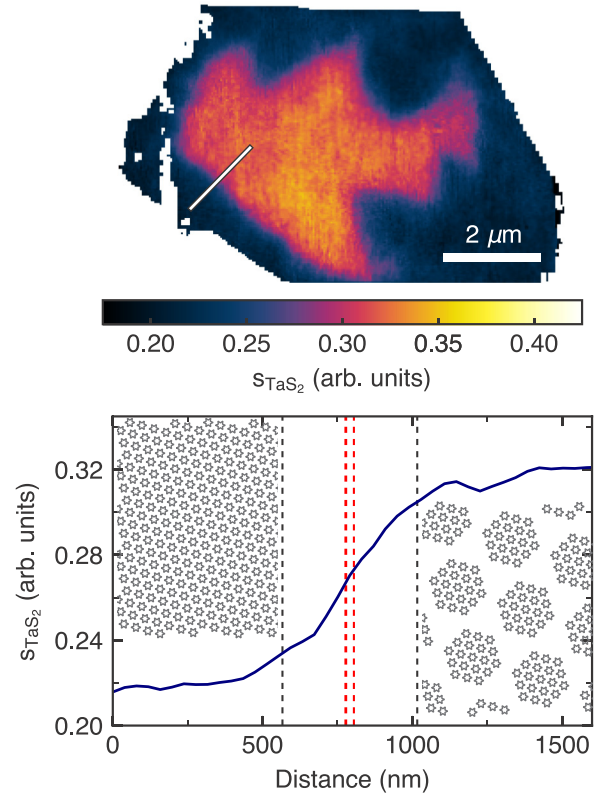

FIG. 3. Domain boundary analysis: (top panel) High-resolution nano-IR image of phase coexistence during the cooling cycle showing the diffuse boundary. (bottom panel) Line cut across the insulator-to-metal boundary (white line in the top panel). The dotted black lines show the fitted FWHM of the transition region ($w \approx 450$ nm), while the dotted red lines show the estimated radius of our AFM tip ($r \approx 27$ nm). Insets: C-CDW (left) and NC-CDW (right) structures. Each star-of-David represents one CDW cluster.

lating phases nearly converge [30,48]. This behavior observed in TaS$_2$ reflects the strong first-order nature of the transition. Examination of the insulating fill fraction [Fig. 2(b), inset] revealed $T_{c,\mathrm{avg}} \approx 185$ K and $\Delta T_c \approx 60$ K, consistent with values obtained on similar samples by transport [31]. While the distributions were bimodal for all temperatures during the transition, the position of the peak for each phase changed as a function of temperature. This peak shift, quantified in Fig. 2(b), was caused by changes of the electronic properties of the respective phases and is not expected within the conventional picture of first-order phase transitions [49].

The observed temperature dependence of the optical properties in the metallic phase of TaS$_2$ may reflect changes to the structure of the NC phase upon cooling. This phase consists of small domains in which the charge-density-wave is commensurate with the atomic lattice (Fig. 3, bottom right inset). These domains are separated by regions in which the CDW is incommensurate, known as discommensurations [2,4,50,51]. The size and periodicity of the commensurate domains have been determined by scanning tunneling microscopy (STM) [4] and transmission electron microscopy [3,31] to change with temperature. For bulk crystals, as the temperature is

lowered, the domain period d increases from $d \approx 70$ Å at room temperature to $d \approx 90$ Å at 200 K. Below 183 K, the CDW becomes fully commensurate with the atomic lattice at the NC-C transition [4]. In thin exfoliated microcrystals such as those we investigated, the NC-C transition temperature is suppressed and the domains reach larger sizes [31].

Our spatial resolution, set by the tip radius $r \approx 27$ nm $\approx 3d$ (Ref. [38]), prevented us from resolving the domains and discommensurations in the NC phase. For the nano-IR signal obtained from each pixel, with area $\approx 75 \times 75$ nm^2, the NC state thus appeared as an effective medium consisting of insulating inclusions in a matrix of conducting domain walls [9,26,31]. The optical response of the effective medium was determined by the optical properties of the insulating domains and metallic discommensurations along with their respective fill fractions [52]. The temperature-dependent domain size set the fill fractions and hence the average conductivity in each pixel, since the discommensuration width is expected to be temperature independent [31,51]. Within this picture, as the temperature was lowered, the insulating domain size within the metallic region increased, which in turn decreased the effective medium conductivity and led to the decreasing nano-IR signal observed in Fig. 2.

We also observed that the nano-IR signal in the insulating regions decreased as temperature was lowered. A similar effect was observed in V_2O_3 (Ref. [30]). In that work, the changes were assigned to temperature dependence of the insulating gap, with the magnitude in the vicinity of the IR frequency employed in the nanoimaging measurements. Similarly, the frequency used in our work was very close to the experimental gap value [53]. Our data therefore admit this tentative interpretation and call for systematic studies of the transition via hyperspectral nanoimaging [54,55]. We note that the temperature dependence of the insulating region properties also influenced the observed changes to the nano-IR signal in the metallic area through the presence of insulating domains. The temperature dependence of s was stronger in the metallic area than in the insulating area, however, and cannot be fully explained by changes to the insulating regions.

Our nanoscale resolution allowed detailed characterization of the boundary region between insulating and metallic areas. A high-resolution nano-IR image of the microcrystal at $T = 155$ K is displayed in the top panel of Fig. 3, exhibiting a gradual transition region between the metallic areas and insulating areas. The bottom panel of Fig. 3 shows a line profile of the phase boundary; the path is indicated by the white line in the top panel. The width of the transition region is much larger than the resolution of our microscope (≈ 27 nm, dashed red lines). Fitting this line profile to a hyperbolic tangent yielded a full-width at half maximum (FWHM) of $w \approx 450$ nm (dashed black lines). Calculation of the boundary FWHM at different temperatures using the images in Fig. 1 revealed that the width did not vary significantly with changing temperature.

This observation of a smooth, wide boundary stands in stark contrast to the metal-insulator boundary observed in STM images of the metastable electrically induced metallic state at low temperature [18,19]. In those works, the transformation between insulating C-CDW state and metastable metallic state occurs over a distance of only ≈ 2.4 nm (two star-of-David clusters), similar to the width of discommensurations observed in the NC state [2]. In the thermodynamic case of our measurements, the phase boundary width is much larger. By analogy with the picture developed to interpret the smooth temperature dependence of s, we hypothesize that the domain structure of the metallic NC phase gradually transitions across the boundary to the C phase, corresponding to a spatially varying C domain size and angle in the discommensuration network. This results in the spatially varying metallicity detected in the nano-IR signal by its local effect on the optical conductivity. The length scale is set by the energy cost of order parameter gradients, an intrinsic property of TaS_2 [49,50]. The continuous spatial variation of the nano-IR signal suggests that the C domain size and ordering in the boundary region may be distinct from what has been observed in the NC state.

To investigate this hypothesis further and offer a microscopic understanding of the spatial transformation between the metallic NC phase and the insulating C phase observed by our nanoimaging, we considered a Ginzburg-Landau (GL)-type theory first proposed by McMillan [56] to describe triple CDWs in transition metal dichalcogenides. In this theory, the thermodynamic free energy F of a crystal monolayer is

expanded in powers of the excess charge density, proportional to an order parameter $\alpha(\mathbf{r}) \equiv \mathrm{Re}\{\psi_1(\mathbf{r}) + \psi_2(\mathbf{r}) + \psi_3(\mathbf{r})\}$. Here, the ψ_i are wave functions representing the charge modulation in three directions rotated from each other by $120°$. Nakanishi *et al.* [50,57] extended this theory to explain the domain structure observed in the NC state by including higher harmonics of the CDW wave vector in the wave functions,

$$\psi_i(\mathbf{r}) = \sum_{l,m,n \leqslant 0} \Delta_{lmn} e^{i \mathbf{Q}_{lmn} \cdot \mathbf{r}}, \qquad (1)$$

where the $\mathbf{Q}_{lmn}$ are characteristic harmonics of the three CDW wave vectors [38]. The thermal evolution of the resulting energetic landscape reflects the phenomenology of CDW transitions in $1T$-TaS_2: while a local energy minimum always exists for the incommensurate wave vector $\mathbf{Q} = \mathbf{Q}_I$, additional minima emerge at temperatures $T < T_c$, first at the nearly commensurate wave vector $\mathbf{Q}_{NC}$ and finally at the commensurate wave vector $\mathbf{Q}_C$. These latter CDW orientations coincide with CDW wavevector angles $\theta_Q \approx 11°$ and $13.9°$ with respect to the crystal a axis, respectively, in accordance with established results [50]. While persistent metastability of these CDW vectors reflects the first-order character of transitions between them, the lowest energy CDW correctly agrees with the thermodynamically favored configuration observed by diffraction and tunneling microscopy measurements of $1T$-TaS_2 (Refs. [2–5]). Notably, the energy barrier between NC and C states is characterized by a non-equilibrium wave vector $\mathbf{Q}_{NE}$ at $\theta_Q \approx 12.5°$, which is not expected to manifest in a homogeneous equilibrium CDW phase, but as we show below, plays an important role at the spatial boundary between NC and C phases.

Within this theoretical framework for CDW order in $1T$-TaS_2, we proceed to examine the expected long-range (compared with the lattice constant) behavior of a phase boundary between coexisting C and NC states. As discerned from Fig. 4(a), both phases are thermodynamically stable at, e.g., $T/T_c = 0.73$. At a spatial boundary between these phases, slow variations (compared with the lattice constant) of the CDW amplitudes $\Delta_{lmn}(\mathbf{r})$ should increase the system free energy F by way of a gradient term in the free energy [49],

$$F_\kappa = \int d^2 \mathbf{r} \left(3 \sum_{l,m,n \geqslant 0} \frac{\kappa}{2} \left| \nabla \Delta_{lmn}(\mathbf{r}) \right|^2 \right). \qquad (2)$$

Here, the factor 3 accounts for triplicate copies of the CDW, and the CDW "stiffness" κ parameterizes the sensitivity of the free energy to slow order parameter variations, i.e., variations with wave vector $|\mathbf{q}| \ll |\mathbf{Q}_I|$. Including the CDW stiffness [Eq. (2)], we have computed the behavior of a one-dimensional intralayer C-NC phase boundary by numerically minimizing the system energy under the condition of coexisting phases at $T/T_c = 0.73$ (Ref. [38]). The result is displayed in Fig. 4(b), which presents the angle θ_Q of the fundamental CDW vector and the characteristic amplitude $\langle \psi \rangle$ of the CDW (Ref. [38]) versus distance x from the phase boundary. The latter is measured against the characteristic length scale ζ of phase coexistence, which follows from microscopic parameters of the theory [38], and bears conceptual resemblance to the coherence length in conventional Ginzburg-Landau theory [49,58].
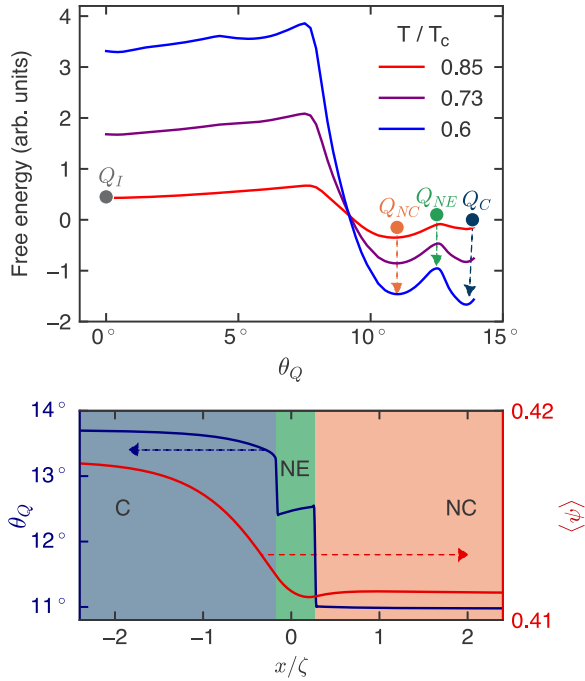
FIG. 4. Nonequilibrium CDW at a phase boundary: (top panel) Landscape of Landau free energy (arbitrary units, relatively offset) minimized for fixed values of $\boldsymbol{Q}$, as identified by their relative angle θ_Q in the Brillouin zone. For $T < T_c$, four distinct phases are metastable as indicated by the colored dots. With decreasing temperature, the $\boldsymbol{Q}$ of lowest energy are $\boldsymbol{Q}_I$, $\boldsymbol{Q}_{NC}$, and $\boldsymbol{Q}_C$, respectively. $\boldsymbol{Q}_{NE}$ denotes a nonequilibrium (NE) CDW state interpolating the NC and C phases (see text). (bottom panel) Numerical minimization of Landau free energy across an inter-phase boundary between C and NC phases. The local orientation of the CDW-vector θ_Q and the local CDW amplitude $\langle \psi \rangle$ are plotted versus distance x from the boundary location, measured in units of ζ, a characteristic length scale [38]. The NE CDW spontaneously stabilizes in proximity to the interphase boundary.

Two noteworthy conclusions follow from the calculation presented in Fig. 4. First, within the theory, the width ζ of the interphase boundary can be identified with the GL coherence length. Our nanoimaging results therefore provide a measure of this correlation length, for which we obtain $\zeta = w \approx 450$ nm. This length, however, is not the same as the zero-temperature CDW coherence length, which is expected to be on the order of the CDW period at low temperature due to the strong-coupling $(2\Delta/k_B T_c \sim 10)$ nature of the CDW in $1T$-TaS$_2$ [6]. In fact, the GL coherence length weakly diverges in proximity to a first-order phase transition [49,58], which may explain the large value observed in our nano-IR measurements. Second, although θ_Q and $\langle \psi \rangle$ both asymptotically reach values associated with the homogeneous equilibrium C and NC phases at $x \to \pm\infty$, respectively, θ_Q does not smoothly interpolate as might be expected. Instead, the CDW vector stabilizes to $\boldsymbol{Q}_{NE}$ over a distance $\delta x \sim \zeta$ centered at the domain boundary. This region at the boundary signifies a nonequilibrium CDW state that is not otherwise energetically favored in any homogeneous state, but is nevertheless thermodynamically metastable at a spatial boundary between C and NC phases.

Our nano-IR observation of intermediate optical conductivities that persist at interphase boundaries provides circumstantial support for the presence of a nonequilibrium CDW order. As discussed above in the context of the observed temperature-dependent nano-IR signal, the size $d \approx 2\pi |\boldsymbol{Q} - \boldsymbol{Q}_C|^{-1}$ of domains in the NC phase (inset of Fig. 3, lower panel) has been identified as a controlling factor in the relative electrical conductivity of the CDW phase [31]. According to this simple paradigm, the local infrared conductivity scales roughly with the angular displacement $\delta\theta_Q(x) \equiv |13.9° - \theta_Q(x)|$, and accordingly the nano-IR response of a putative nonequilibrium CDW at $\boldsymbol{Q} = \boldsymbol{Q}_{NE}$ should be expected to reach about half that of the NC state, helping to explain the long-range interpolation of optical conductivity we experimentally observe at interphase boundaries. Observations of nonequilibrium CDW phases have been claimed in previous studies, but these proposed states have been accessed only under the action of strong extrinsic stimuli, such as nanosecond voltage pulses and ultrafast laser excitation [13–19]. In contrast, our nanoimaging study motivates further nanoresolved study of nonequilibrium CDW phases already thermodynamically accessible in $1T$-TaS$_2$, with particular attention to the electronic structure at CDW interphase boundaries.

IV. CONCLUSION

Our infrared nanoimaging experiments revealed a rich mesoscopic electronic phase behavior and emergent length scales previously unobserved in $1T$-TaS$_2$. Our analysis suggests the presence of new intermediate electronic states, which could be observed by atomic-resolution measurements on similar thin exfoliated samples. These results lay the foundation for future work exploring mesoscale real-space features of the MIT as a function of microcrystal thickness [31,33,59,60]. Additionally, because infrared nanoimaging is an all-optical technique, pump-probe methods may be used to probe transient polaronic states [61], as well as metastable states induced by light [13] or electrical perturbation [15,16]. Such experiments would provide an unprecedented glimpse into the mesoscopic texture of these transient and metastable states. Additionally, inducing these metastable states at a variety of temperatures and performing nano-IR measurements over mesoscopic length scales may allow to extract the temperature dependence of the GL correlation length and hence further characterize the microscopic parameters of the Ginzburg-Landau theory.

[1] J. A. Wilson, F. J. Di Salvo, and S. Mahajan, Adv. Phys. **24**, 117 (1975).

[2] X. L. Wu and C. M. Lieber, Science **243**, 1703 (1989).

[3] T. Ishiguro and H. Sato, Phys. Rev. B **44**, 2046 (1991).

[4] R. E. Thomson, B. Burk, A. Zettl, and J. Clarke, Phys. Rev. B **49**, 16899 (1994).

[5] A. Spijkerman, J. L. de Boer, A. Meetsma, G. A. Wiegers, and S. van Smaalen, Phys. Rev. B **56**, 13757 (1997).

[6] K. Rossnagel, J. Phys. Condens. Matter **23**, 213001 (2011).

[7] S. Yan, D. Iaia, E. Morosan, E. Fradkin, P. Abbamonte, and V. Madhavan, Phys. Rev. Lett. **118**, 106405 (2017).

[8] E. Morosan, H. W. Zandbergen, B. S. Dennis, J. W. G. Bos, Y. Onose, T. Klimczuk, A. P. Ramirez, N. P. Ong, and R. J. Cava, Nat. Phys. **2**, 544 (2006).

[9] B. Sipos, A. F. Kusmartseva, A. Akrap, H. Berger, L. Forró, and E. Tutiš, Nat. Mater. **7**, 960 (2008).

[10] L. J. Li, W. J. Lu, X. D. Zhu, L. S. Ling, Z. Qu, and Y. P. Sun, Europhys. Lett. **97**, 67005 (2012).

[11] Y. Liu, R. Ang, W. J. Lu, W. H. Song, L. J. Li, and Y. P. Sun, Appl. Phys. Lett. **102**, 192602 (2013).

[12] E. Navarro-Moratalla, J. O. Island, S. Mañas-Valero, E. Pinilla-Cienfuegos, A. Castellanos-Gomez, J. Quereda, G. Rubio-Bollinger, L. Chirolli, J. A. Silva-Guillén, N. Agraït, G. A. Steele, F. Guinea, H. S. J. van der Zant, and E. Coronado, Nat. Commun. **7**, 11043 (2016).

[13] L. Stojchevska, I. Vaskivskyi, T. Mertelj, P. Kusar, D. Svetin, S. Brazovskii, and D. Mihailovic, Science **344**, 177 (2014).

[14] T.-R. T. Han, F. Zhou, C. D. Malliakas, P. M. Duxbury, S. D. Mahanti, M. G. Kanatzidis, and C.-Y. Ruan, Sci. Adv. **1**, e1400173 (2015).

[15] M. Yoshida, R. Suzuki, Y. Zhang, M. Nakano, and Y. Iwasa, Sci. Adv. **1**, e1500606 (2015).

[16] M. J. Hollander, Y. Liu, W. J. Lu, L.-J. Li, Y.-P. Sun, J. A. Robinson, and S. Datta, Nano Lett. **15**, 1861 (2015).

[17] I. Vaskivskyi, I. A. Mihailovic, S. Brazovskii, J. Gospodaric, T. Mertelj, D. Svetin, P. Sutar, and D. Mihailovic, Nat. Commun. **7**, 11442 (2016).

[18] L. Ma, C. Ye, Y. Yu, X. F. Lu, X. Niu, S. Kim, D. Feng, D. Tománek, Y.-W. Son, X. H. Chen, and Y. Zhang, Nat. Commun. **7**, 10956 (2016).

[19] D. Cho, S. Cheon, K.-S. Kim, S.-H. Lee, Y.-H. Cho, S.-W. Cheong, and H. W. Yeom, Nat. Commun. **7**, 10453 (2016).

[20] E. Tosatti and P. Fazekas, J. Phys. **37**, 165 (1976).

[21] J.-J. Kim, W. Yamaguchi, T. Hasegawa, and K. Kitazawa, Phys. Rev. Lett. **73**, 2103 (1994).

[22] P. Kim, J. Zhang, and C. M. Lieber, Solid State Phys. **55**, 119 (2001).

[23] G. Liu, B. Debnath, T. R. Pope, T. T. Salguero, R. K. Lake, and A. A. Balandin, Nat. Nanotechnol. **11**, 845 (2016).

[24] M. Imada, A. Fujimori, and Y. Tokura, Rev. Mod. Phys. **70**, 1039 (1998).

[25] L. Zhang, C. Israel, A. Biswas, R. L. Greene, and A. de Lozanne, Science **298**, 805 (2002).

[26] M. M. Qazilbash, M. Brehm, B.-G. Chae, P.-C. Ho, G. O. Andreev, B.-J. Kim, S. J. Yun, A. V. Balatsky, M. B. Maple, F. Keilmann, H.-T. Kim, and D. N. Basov, Science **318**, 1750 (2007).

[27] K. Lai, M. Nakamura, W. Kundhikanjana, M. Kawasaki, Y. Tokura, M. A. Kelly, and Z.-X. Shen, Science **329**, 190 (2010).

[28] M. K. Liu, M. Wagner, E. Abreu, S. Kittiwatanakul, A. McLeod, Z. Fei, M. Goldflam, S. Dai, M. M. Fogler, J. Lu, S. A. Wolf, R. D. Averitt, and D. N. Basov, Phys. Rev. Lett. **111**, 096602 (2013).

[29] E. Y. Ma, Y.-T. Cui, K. Ueda, S. Tang, K. Chen, N. Tamura, P. M. Wu, J. Fujioka, Y. Tokura, and Z.-X. Shen, Science **350**, 538 (2015).

[30] A. S. McLeod, E. van Heumen, J. G. Ramirez, S. Wang, T. Saerbeck, S. Guenon, M. Goldflam, L. Anderegg, P. Kelly, A. Mueller, M. K. Liu, I. K. Schuller, and D. N. Basov, Nat. Phys. **13**, 80 (2016).

[31] A. W. Tsen, R. Hovden, D. Wang, Y. D. Kim, J. Okamoto, K. A. Spoth, Y. Liu, W. Lu, Y. Sun, J. C. Hone, L. F. Kourkoutis, P. Kim, and A. N. Pasupathy, Proc. Natl. Acad. Sci. USA **112**, 15054 (2015).

[32] R. Hovden, A. W. Tsen, P. Liu, B. H. Savitzky, I. El Baggari, Y. Liu, W. Lu, Y. Sun, P. Kim, A. N. Pasupathy, and L. F. Kourkoutis, Proc. Natl. Acad. Sci. USA **113**, 11420 (2016).

[33] D. Sakabe, Z. Liu, K. Suenaga, K. Nakatsugawa, and S. Tanda, npj Quantum Mater. **2**, 22 (2017).

[34] B. Knoll and F. Keilmann, Nature **399**, 134 (1999).

[35] J. M. Atkin, S. Berweger, A. C. Jones, and M. B. Raschke, Adv. Phys. **61**, 745 (2012).

[36] M. A. Huber, M. Plankl, M. Eisele, R. E. Marvel, F. Sandner, T. Korn, C. Schüller, R. F. Haglund, Jr., R. Huber, and T. L. Cocker, Nano Lett. **16**, 1421 (2016).

[37] M. Liu, A. J. Sternbach, and D. N. Basov, Reports Prog. Phys. **80**, 014501 (2017).

[38] See Supplemental Material at http://link.aps.org/supplemental/10.1103/PhysRevB.97.035111, which includes Refs. [39–44], for additional data and further details of the experimental setup, lightning-rod model, and Ginzburg-Landau theory.

[39] N. Ocelic, A. Huber, and R. Hillenbrand, Appl. Phys. Lett. **89**, 101124 (2006).

[40] A. Kučírková and K. Navrátil, Appl. Spectrosc. **48**, 113 (1994).

[41] A. B. Kuzmenko, Rev. Sci. Instrum. **76**, 083108 (2005).

[42] L. M. Zhang, G. O. Andreev, Z. Fei, A. S. McLeod, G. Dominguez, M. Thiemens, A. H. Castro-Neto, D. N. Basov, and M. M. Fogler, Phys. Rev. B **85**, 075419 (2012).

[43] S. Dai, Z. Fei, Q. Ma, A. S. Rodin, M. Wagner, A. S. McLeod, M. K. Liu, W. Gannett, W. Regan, K. Watanabe, T. Taniguchi, M. Thiemens, G. Dominguez, A. H. Castro Neto, A. Zettl, F. Keilmann, P. Jarillo-Herrero, M. M. Fogler, and D. N. Basov, Science **343**, 1125 (2014).

[44] A. Logg, Arch. Comput. Methods Engin. **14**, 93 (2007).

[45] A. S. McLeod, P. Kelly, M. D. Goldflam, Z. Gainsforth, A. J. Westphal, G. Dominguez, M. H. Thiemens, M. M. Fogler, and D. N. Basov, Phys. Rev. B **90**, 085136 (2014).

[46] M. Born and E. Wolf, *Principles of Optics*, 7th ed. (Cambridge University Press, Cambridge, 1999).

[47] D. Svetin, I. Vaskivskyi, P. Sutar, E. Goreshnik, J. Gospodaric, T. Mertelj, and D. Mihailovic, Appl. Phys. Express **7**, 103201 (2014).

[48] M. M. Qazilbash, M. Brehm, G. O. Andreev, A. Frenzel, P.-C. Ho, B.-G. Chae, B.-J. Kim, S. J. Yun, H.-T. Kim, A. V. Balatsky, O. G. Shpyrko, M. B. Maple, F. Keilmann, and D. N. Basov, Phys. Rev. B **79**, 075107 (2009).

[49] M. Sanati and A. Saxena, Am. J. Phys. **71**, 1005 (2003).

[50] K. Nakanishi and H. Shiba, J. Phys. Soc. Japan **43**, 1839 (1977).

[51] X. L. Wu and C. M. Lieber, Phys. Rev. Lett. **64**, 1150 (1990).

[52] G. L. Carr, S. Perkowitz, and D. B. Tanner, in *Infrared and Millimeter Waves*, edited by K. J. Button (Academic Press, Orlando, 1985), Vol. 13, pp. 171–263.

[53] L. V. Gasparov, K. G. Brown, A. C. Wint, D. B. Tanner, H. Berger, G. Margaritondo, R. Gaál, and L. Forró, Phys. Rev. B **66**, 094301 (2002).

[54] G. Dominguez, A. S. Mcleod, Z. Gainsforth, P. Kelly, H. A. Bechtel, F. Keilmann, A. Westphal, M. Thiemens, and D. N. Basov, Nat. Commun. **5**, 5445 (2014).

[55] I. Amenabar, S. Poly, M. Goikoetxea, W. Nuansing, P. Lasch, and R. Hillenbrand, Nat. Commun. **8**, 14402 (2017).

[56] W. L. McMillan, Phys. Rev. B **12**, 1187 (1975).

[57] K. Nakanishi, H. Takatera, Y. Yamada, and H. Shiba, J. Phys. Soc. Japan **43**, 1509 (1977).

[58] M. Tinkham, *Introduction to Superconductivity*, 2nd ed. (Dover, Mineola, 2004).

[59] M. Yoshida, Y. Zhang, J. Ye, R. Suzuki, Y. Imai, S. Kimura, A. Fujiwara, and Y. Iwasa, Sci. Rep. **4**, 7302 (2014).

[60] Y. Yu, F. Yang, X. F. Lu, Y. J. Yan, Y.-H. Cho, L. Ma, X. Niu, S. Kim, Y.-W. Son, D. Feng, S. Li, S.-W. Cheong, X. H. Chen, and Y. Zhang, Nat. Nanotechnol. **10**, 270 (2015).

[61] N. Dean, J. C. Petersen, D. Fausti, R. I. Tobey, S. Kaiser, L. V. Gasparov, H. Berger, and A. Cavalleri, Phys. Rev. Lett. **106**, 016401 (2011).